Journal of Molecular Structure 1298 (2024) 136979

Contents lists available at ScienceDirect

Journal of Molecular Structure

journal homepage: www.elsevier.com/locate/molstr

Biophysical characterization, crystallization, and solution of the first crystal structure of the 28 kDa-*Schistosoma bovis* glutathione transferase

Hattie Hope Makumbe, Ramesh Pandian, Akeel Valli, Yasien Sayed, Ikechukwu Achilonu *

Protein Structure-Function Research Unit, School of Molecular and Cell Biology, Faculty of Science, University of the Witwatersrand, Gatehouse, 4th Floor, 1 Jan Smuts Avenue, 2000, Braamfontein, Johannesburg, South Africa

ARTICLE INFO

Keywords:
Schistosoma bovis
B-factor
28-kDa glutathione transferase
Apoenzyme
X-ray crystallography

ABSTRACT

Glutathione *S*-transferase (GST) is a potential therapeutic drug target against helminthic diseases. This essential enzyme prevents oxidative stress by inhibiting the toxic build-up of xenobiotics in the worm during human host infection. *Schistosoma* schistosome manifests two GST isoforms, namely the 26- and 28-kDa GST, which exhibit contrasting substrate specificities within the worm. This study was designed to explore the structural and functional relationships of *Schistosoma bovis* 28 kDa-GST (Sb28GST) through crystallographic studies. The 1-Chloro-2,4-Dinitrobenzene-Glutathione assay revealed that the enzyme was catalytically active. The secondary structural content confirmed that Sb28GST follows a canonical GST fold, mostly alpha-helical. Extrinsic 1-anilinonaphthalene-8-sulfonic acid substitution revealed buried hydrophobic clefts within the enzyme. Sb28GST was purified by immobilised metal affinity chromatography. Crystal structures of Sb28GST were determined for the un-ligated enzyme (resolution = 2.3 Å, R_{factor} = 21.68 %). The crystals belonged to the monoclinic space group $P2_1$, which accommodated two biological molecules in the asymmetric unit with the unit-cell parameters of a = 54.133, b = 77.086, c = 54.015 Å and β = 93.15° Computational modelling studies predicted the catalytic propensity of 8ALS may vary from that of 1OE8 by differences in the molecular dynamic trajectory, especially at the dimer interface of this obligate dimeric enzyme.

1. Introduction

Human Schistosomiasis (Bilharzia) is a neglected, detrimental, tropical and poverty-associated disease caused by trematode parasites from the *Schistosoma* genus. The disease is responsible for the debilitating health conditions of over 240 million infected people [1]. The intermediate human and freshwater snail host maintains the schistosome life cycle. The Schistosome parasite exhibits different life stages within the host where the parasite acquires host immune system evasion strategies—three major *Schistosoma* parasites (*Schistosoma mansoni, Schistosoma japonicum*, and *S. haematobium*).

The Glutathione transferase (GST) superfamily is divided into three broad categories: membrane-associated proteins, mitochondrial GSTs and cytosolic GSTs, with the latter being the most abundant and pharmacologically significant [2–5]. The "C" terminal of GSTs is predominantly alpha-helical, while the selective "N" terminal exhibits an alternating α-helix and β-strand topology. The active site consists of a hydrophobic co-substrate known as the "H-site" and a GSH binding site "G-site" [6]. Furthermore, various forms of GSTs have been identified to possess a non-substrate binding site in the enzyme core adjoining the "G-site" and "H-site". This binding site forms the interface of the GST dimer and is commonly implicated in drug binding (Fig. 5). Differences amongst GSTs include variations in the structure and chemistry of the "H" site between the various classes [7], and such variability makes ligand binding possible. To date, the alpha (σ), mu (μ), and pi (π) kappa, omega, theta and zeta GST classes are well categorised amongst cytosolic GSTs in mammals [8]. The Sb28GST under investigation in this study originates from the Sigma class. The sequences of various GST classes exhibit a low similarity index despite showing identical folding in virtually all the recorded three-dimensional GST structures [9].

The primary function of GST is to detoxify pathogenic cells of helminths that cause schistosomiasis [10–12]. Detoxification is achieved by catalysing the reduced glutathione. In addition, GSTs possess ligandin capabilities and bind to numerous electrophiles, posing as plausible

Funding: This work was supported by the University of the WitwatersrandJournal policies detailed in the Journal of Molecular Structure Guide have been reviewed.
Consent for publication: All authors consent to the publication of this manuscript.
* Corresponding authors.
E-mail address: Ikechukwu.Achilonu@wits.ac.za (I. Achilonu).

https://doi.org/10.1016/j.molstruc.2023.136979
Received 5 May 2023; Received in revised form 18 October 2023; Accepted 1 November 2023

schistosomiasis drug and vaccine targets [13]. It is assumed that there is dormant detoxification, which GSTs induce in anti-helminthic drugs [14,15]. Drug design efforts have focused on Praziquantel, whose mode of action is poorly understood [16]. The GSTs also function in chemotherapy resistance [17], thus making them potential drug targets for chemotherapy [9]. GSTs possess ligandin functionalities since they can bind xenobiotics in a non-covalent manner [18]. The ligandin functionality was named after the promiscuous binding of various non-substrate ligands, such as bilirubin [19]. This ligandin activity is known to result in the suppression of catalytic activity [20]. Future promising drug targets against schistosomiasis should inhibit the catalytic activity of GSTs, thereby detoxifying the electrophilic substrates [13].

There has never been any published crystal structure of the 28 kDa-*Schistosoma bovis* GST (Sb28GST), even though this enzyme is at variance with the 28 kDa-*Schistosoma haematobium* GST at six amino acid positions. This study reports the first case of an apo-crystal form of the Sb28GST enzyme. Characterising an enzyme's apo state is the basis for designing small molecule soaking and co-crystallisation experiments [21]. Ligand binding is known to induce numerous structural changes in a protein. This postulate is supported by several studies on GSTs in solution, which have revealed massive conformational changes [22–24]. Analysis of apo and holo-enzyme forms is crucial in understanding protein binding functionality. In this current study, unliganded crystal structures of Sb28GST were solved at a molecular level to interpret the protein's interaction, function and structure. Dealing with compounds at the molecular level is essential for revealing the intricacies of drug discovery. This present study aims to enclose the current research gap in the structure and function of Sb28GST.

2. Experimental procedure

2.1. Materials

All chemicals and reagents were of analytical grade. Vector synthesis was done by GenScript (NJ, USA). Crystal screening buffers, reagents and other apparatus were purchased from Hampton Research (CA, USA). Purchases from Sigma-Aldrich (MO, USA) included reagents such as Coomassie Blue-G250 dye, antibiotics (chloramphenicol and ampicillin), 2xYT, Glutathione-agarose resin, Isopropyl β-d-1 thiolgalactopyranoside (IPTG), BLUeye prestained protein ladder, BSP, l-glutathione and 1-Chloro-2,4-Dinitrobenzene (CDNB). In contrast, the ANS was procured from the local Sigma-Aldrich (South Africa). The *Escherichia coli* (*E. coli*) T7 Express chemically competent cells were procured from New England Biolabs (USA). The 15-well EasyXtal® plates were purchased from Qiagen.

2.2. Protein expression and purification

The full-length nucleotide sequence of Sb28GST was extracted from UniProtKB (P30114) linked ENA sequence AAA29893 (EMBL), which codes for full-length *Schistosoma bovis* 28-kDa glutathione transferase. The sequence was modified to encode an N-terminal hexahistidine tag, an *Nde*I and a *BamH*I endonuclease restriction sites for cloning into pET11a (+) vector by GenScript Corporation (NJ, USA). The pET11a (+) vector included an ampicillin resistance gene as a selectable marker. Cloning was done by restriction enzymes. The 5′ sequencing primer consisted of T7, whilst the 3′ sequencing primer consisted of a T7-terminal. The vector also possesses an f1 origin of replication for sequencing and mutagenesis purposes. The C-and N-terminal hexahistidine tag facilitated metal chelation purification.

Expression of recombinant Sb28GST was performed using the protocol which has been previously described [25]. However, in this work, 0.5 mM IPTG was used to induce the overexpression of Sb28GST in *E. coli* T7 Expression cells. Protein purification was accomplished by immobilised Ni^{2+}-affinity chromatography. The protein concentration was determined spectrophotometrically to be approximately ~5.3 mg/mL. The purity and homogeneity of the purified protein were determined using Sodium Dodecyl Sulphate-Polyacrylamide Gel Electrophoresis (SDS-PAGE). The concentration of the purified Sb28GST was estimated spectroscopically by use of the Beer-Lambert law:

$$A_{280} = \varepsilon \cdot c \cdot l \quad (1)$$

where A280 is the absorption value obtained at 280 nm, ε is the molar extinction coefficient ($M^{-1}cm^{-1}$) at 280 nm, c is the concentration (M) value to be determined, and l is the cell path length (cm). The molar extinction coefficient for Sb28GST was determined using the Expasy ProtParam tool [26].

2.3. Protein characterisation

2.3.1. Specific activity assay for Sb28GST

The specific activity of Sb28GST was determined by the CDNB glutathione conjugation activity assay [27,28]. Conjugation of CDNB with GSH was analysed by recording the change in absorbence for a minute at 340 nm. A total of three replicates of concentrations of 10 – 50 nM of Sb28GST were assayed in a reaction mixture containing 100 mM NaH_2PO_4 consisting of 0.02 % (w/v) NaN_3, 1 mM Ethylenediaminetetraacetic acid (EDTA), 2 mM Dithiothreitol (DTT) and 1 mM GSH, pH 6.5 to which 1 mM of CDNB was added. The Jasco V-550 UV/Vis spectrophotometer was used to measure the product's (1-(*S*-glutathionyl)−2,4-dinitrobenzene) appearance. The slope from the linear regression curve was used to depict the reaction rate.

2.3.2. Far-UV circular dichroism

The secondary structure content of Sb28GST was performed with far-UV circular dichroism (far-UV CD) by use of a Jasco J-1500 spectropolarimeter with Spectra Manager software v1.5.00 (Jasco Inc., Tokyo, Japan). Samples of 2 μM of the protein were prepared in 20 Mm NaH_2PO_4, pH 7.5, and 0.02 % (w/v) NaN_3. All spectra measurements were taken at 293 K with a bandwidth of 5 nm, a scan speed of 200 nm/min, a data pitch of 1 nm, and a 1-second response time for ten accumulations between 185 and 245 nm. The data was buffer-corrected and adjusted from millidegrees to mean residue ellipticity [θ] ($deg.cm^2.dmol^{-1}$).

2.3.3. Intrinsic fluorescence

The 3-dimensional structure of Sb28GST was analysed through intrinsic Tryptophan fluorescence by either including or excluding GSH. A Jasco FP-6300 spectrofluorometer with Spectra Manager software v1.5.00 (Jasco Inc., Tokyo, Japan) was used to measure the spectra at 293 K in triplicate. The samples either included or excluded GSH with a 10 μM Sb28GST concentration. Further, incubation in NaH_2PO_4, pH 7.5, 1 mM DTT, 1 mM EDTA and 0.02 % (w/v) NaN_3 occurred over a 30-minute time frame by including or excluding GSH at 100 μM. Fluorescence took place between 250 and 500 nm with fifteen accumulations at a 1 cm pathlength, emission and excitation bandwidth of 5 nm, data pitch of 1 nm, scanning speed of 200 nm/min, and excitation at 295 nm.

2.3.4. Extrinsic ANS fluorescence

Hydrophobic clefts were probed using extrinsic ANS fluorescence. The signal was monitored from 395 to 650 nm with fifteen accumulations at 1 cm path length, excitation bandwidth of 5 nm and emission of 5 nm, data pitch of 1 nm, scanning speed of 200 nm/min, and excitation at 395 nm. Spectra from the replicates were averaged and buffer corrected.

2.3.5. Protein crystallisation

The purified Sb28GST was dialysed against 25 mM NaH_2PO_4 buffer. Crystals of Sb28GST (apo form) were produced in hanging drops and set up in 15-well Xtal Easy™ crystallisation plates. The mother liquor

solution consisted of 2.1 M ammonium sulphate, 100 mM Tris (pH 7.5), and 5 mM β-mercaptoethanol. Each hanging drop (5 μL) was prepared by mixing the stock protein solution [231 μM- 5.3 mg/mL] in NaH_2PO_4 with the reservoir solution in a ratio of 1: respectively. Large diffractive needle-shaped crystals grew within two days.

2.4. X-ray diffraction and data processing

The Sb28GST crystal was mounted in a nylon loop and then transferred to a universal cryoprotectant paratone (Parabar 10,312; Hampton Research) solution used as the cryoprotectant before being flash-frozen in liquid nitrogen at 100 K. X-ray crystallographic data for Sb28GST were collected on a Bruker D8 Venture Bio PHOTON III 28-pixel array area detector (208 × 128 mm^2) diffractometer with a Cu Kα IμS DIAMOND source (50 kV, 1.2 mA). The unit cell and full data set were collected using PROTEUM4: SAINT was used to integrate the data, and SADABS was used to make empirical absorption corrections and scale the data [29]. The diffraction data were processed using the SCALEPACK and AIMLESS/POINTLESS inbuilt in the PROTEUM4 software suite [29–32]. Structural solution was done by using the Molecular replacement method using PHASER program built in PHENIX software [33] using 28-kDa glutathione transferase from *Schistosoma haematobium* (glutathione saturated) with the PDB ID: 1OE8 as a starting model. Model building was constructed with the WinCoot Program [34]. During refinement, the water molecules were identified in the difference Fourier using the "Flat Bulk Solvent Model" procedure within Coot. The distance criteria of 2.21 Å to 3.5 Å were applied to the protein structure. After that, further refinement of the protein structure was done using PHENIX [35]. The structure validation of the refined model was performed using PROCHECK [36]. The PyMOL software (Schrödinger LLC., Portland, USA) was used to generate images of the structure.

2.5. Molecular modelling studies

2.5.1. Computer hardware

All molecular modelling studies were performed on two high-performance gaming computing units with the following configurations: the Maestro algorithm was installed in a Windows OS PC containing an AMD RYZEN Threadripper 1950X Processor, Asus Rog Strix X399-E Gaming Ryzen AMD with 40 MB of Cache Memory, 4 TB drive 6GB/s 3D NAND internal SSD with 560 MB/s read, 520 MB/s write, a 4.0 GHz Precision Boost (up to 4.2 GHz) X399 chipset, Quad-Channel DDR4, motherboard, 64GB (16GB x 4) 3200 MHz DDR4 desktop gaming RAM and MSI GeForce RTX 2080 Ti 11 GB GDDR6 4352 CUDA core graphics card. The Desmond molecular dynamics simulation algorithm was installed in an Ubuntu OS PC containing an AMD Threadripper 3990 × 4.3 GHz GT 1030 2 GB PRO high-performance workstation (288 MB Cache, 64x Cores, 4.3 GHz Turbo) with an MSI TRX40 PRO 10 G AMD Ryzen Threadripper motherboard, a GeForce RTX 2070 8GB GDDR6 graphics card a 3200 MHz 64GB gaming RAM, 1 TB M.2 SSD with up to 3.5 GB/s speed, and a 4 TB HDD.

2.5.2. Preparation of molecular systems

The coordinates of the crystal structure of *Schistosoma haematobium* GST in complex with GSH (1OE8) was extracted from RCSB-PDB and the *Schistosoma bovis* 28-kDa GST solved in-house (RCSB-PDB ID: 8ALS, unreleased) were subjected to energy minimisation using OPLS_2005 implemented in the Protein Preparation wizard algorithm of Maestro v13.0. Two molecular systems (Apo-8ALS and Apo-1OE8) were primarily prepared for molecular dynamic simulation calculation by creating a solvated system containing counter charges in a 0.15 M NaCl system using the System Builder implemented in Maestro v13.0. Each molecular system was briefly imported into the System Builder tool in Maestro. The following parameters were used to build each molecular system using the OPLS_2005 force field: (i) TIP3P solvent model, which specifies a three-site rigid water molecule with charges and Lennard-Jones parameters assigned to each three atoms of the water molecule, (ii) orthorhombic periodic boundary box (box condition; distances from the box boundary (Å): $a = 10 \times b = 10 \times c = 10$ and angles: $\alpha = 90° \times \beta = 90° \times \gamma = 90°$) and minimising the volume, (iii) counter ions (Na^+ or Cl^-) were added according to the overall charge of each molecular system a model system and (iv) finally the systems were conditioned to have 0.15 M NaCl. Each system was saved as a *.mae* file and submitted to the Desmond molecular dynamics simulation engine for molecular dynamic simulation.

2.5.3. Molecular dynamic simulation

Briefly, the solvated neutralised molecular systems were subjected to molecular dynamic simulations, employing the ensemble parameter [NPT: isothermal-isobaric ensemble, Number of particles (N), Pressure (P) and Temperature (T)], at 300 K temperature, and 1 bar pressure. The RESPA (reference system propagator algorithms) integrator was used to accelerate simulations of the molecular systems with a separation of time scales (bonded forces: 2 fs, near-range nonbonded forces: 2 fs and far-range non-bonded forces: 6 fs). The Nosé-Hoover chain thermostat method was employed to maintain a stable temperature at 300 K with a relaxation time of 1 ps. In contrast, the Martyna-Tobias-Klein barostat method was used to keep the pressure of the molecular systems at ~ 1 atm with a relaxation time of 2 ps and isotropic coupling style. Short-range coulombic interactions were treated using the cutoff method (cutoff radius = 9 Å). The production phase of the molecular dynamic simulation run time was 500 ns, and the molecular systems were relaxed using the default relaxation protocol implemented in the Desmond algorithm. The MDS phase was divided into eight distinct stages in which the simulation parameters were specified for each stage. Stages 1–7 is the equilibration, which comprises short simulation steps involving a 100 ps simulation carried out (at stage 2) using Brownian Dynamics under NVT condition at 10 K with restraints placed on the solute heavy atoms. The final stage is the long-range 500 ns simulation stage.

2.5.4. Post-dynamic analysis

Following the MD simulation, post-dynamic analyses of the trajectories derived from the MD simulation studies were carried out using Maestro v13.0 for comparative analysis of the conformational dynamics of the two molecular systems. Basically, (i) the simulation quality which analyses the average energy, pressure, temperature, and volume of each simulated system were evaluated using Simulation Quality Analysis (implemented in Maestro v13.0). (ii) The root-mean-square-deviation (RMSD) of the alpha carbon atoms (Cα) and the root-mean-square fluctuations (RMSF) of the residues. The radius of gyration (Rg) and atomic distance calculations were performed using the Simulation Events Analysis tool (also implemented in Maestro v13.0). The average of a representative cluster was determined using the Cα RMSD trajectory cluster analysis algorithm (implemented in Maestro v 13.0).

3. Results

3.1. Expression and purification

Clustal Omega (https://www.ebi.ac.uk/Tools/msa/clustalo/) was used to align the sequences obtained from the Genbank. Protein synthesis proceeded based on the provided sequence and yielded much more accurate and favourable results. Expression yielded a wet cell pellet of approximately 4.5 g/L of culture. Analysis of the SDS-PAGE (Fig. 1) reveals an outstanding soluble protein yield. The Sb28GST monomer showed a molecular weight of about 24 kDa, corresponding to each polypeptide's theoretical subunit weight [26].

3.2. Sb28GST enzyme activity assay

In this assay, the specific activity of the enzyme was calculated using an extinction coefficient of 9600 $M^{-1}.cm^{-1}$ for 1-(*S*-glutathionyl)−2,4-

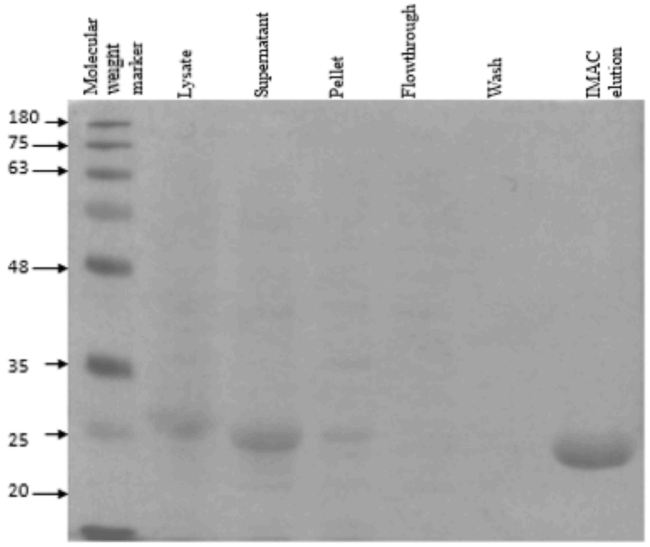

Fig. 1. Expression and purification profile. A 12.5 % (w/v) polyacrylamide gel of the non-liganded 28 kDa *Schistosoma* glutathione transferase [containing 10 % (w/v) SDS], perceivable with Coomassie brilliant blue staining.

dinitrobenzene [18]. The reaction rate in the absence of GSH (substrate) was recorded. However, the results were negligible. The specific activity of Sb28GST was reported to be 14 μmol/min/mg with an R^2 value of 0, 9755. Sb28GST exhibited high transferase activity with CDNB. The error bar shows the standard deviation. The experimental data was buffer-corrected.

3.3. Far-UV circular dichroism

The peptide bonds of Sb28GST served as a chromophore in the far-UV region based on their capability to polarise light. Far-UV circular dichroism (far-UV CD) was used to analyse the secondary structure content of Sb28GST in the presence or absence of GSH. Data was buffer-corrected and normalised from millidegrees to mean residue ellipticity - [Θ] (deg.cm^2.dmol^{-1}) according to the following equation:

$$[Q] = 100 \times \theta / cnl \quad (3)$$

Where, θ is the CD signal in millidegrees, c is the protein concentration in mM, n is the number of residues, and l is the path length (cm). The resulting CD spectra showed a peak of positive ellipticity at 195 ± 0.5 nm and two troughs with a negative ellipticity at 222 ± 0.5 nm and 208 ± 0.5 nm, (Fig. 2B), a profile typical of predominantly alpha-helical proteins. CD spectra readings in the presence of GSH yielded readings that are not different from those without GSH. The deconvolution of the CD spectra data into the corresponding secondary structure content was done via the DichroWeb analysis program [37].

3.3.1. X-ray crystallography

Crystals of Sb28GST were obtained (Fig. 3A) by the hanging drop vapour diffusion method. The PHASER program (with incorporated

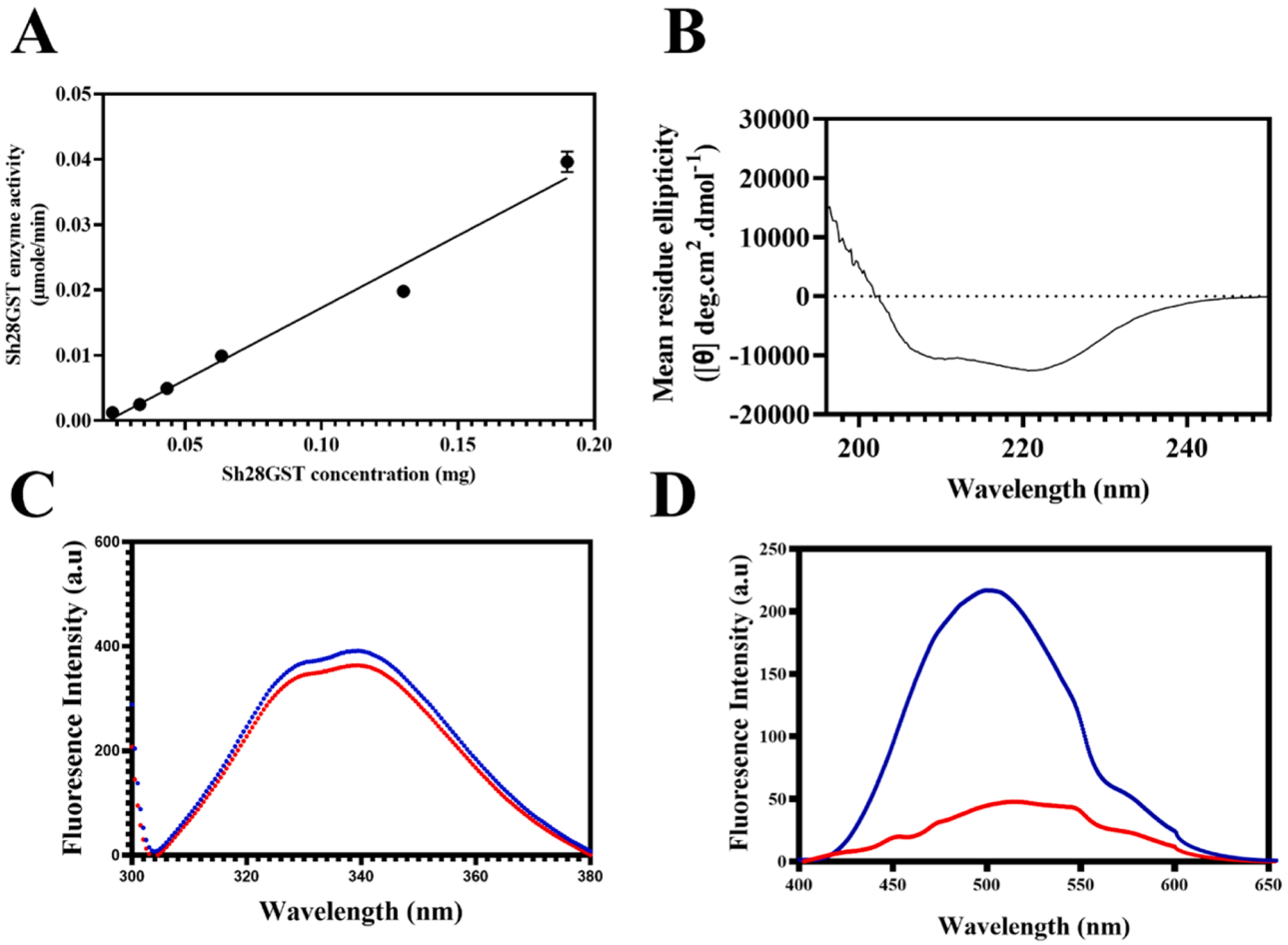

Fig. 2. Structural characterisation studies. (*A*) CDNB-GSH conjugation assay for determination of the specific activity of Sb28GST. (*B*) The secondary structure of Sb28GST. (*C*) Intrinsic tryptophan fluorescence emission spectra of Sb28GST concentration (*D*) Extrinsic ANS fluorescence spectra of Sb28GST. Extrinsic ANS fluorescence spectra of unbound ANS (red line), ANS bound to Sb28GST (blue line).

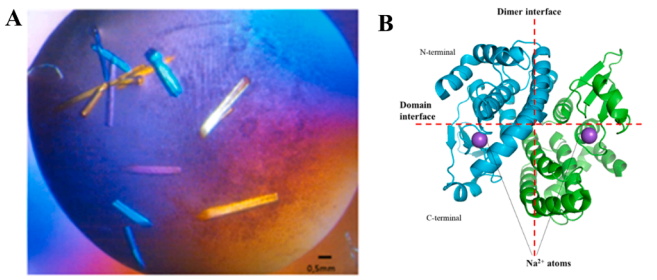

Fig. 3. (*A*) Sb28GST crystals. (*B*) Ribbon representation of the non-liganded Sb28GST. The structure contains two subunits (green) and a sodium atom (red). The ribbon diagram was generated using the PyMol molecular graphics program.

PHENIX algorithm) was used for molecular replacement [38]. The presence of the sodium atom (Fig. 4A) is warranted since the crystallisation buffer contained sodium phosphate within the precipitation buffer. The structure was refined with a final R_{factor} of 18.7% at 1.53 Å resolution with a solvent content of 48.1 % (Table 1). Matthew's coefficient (V_M) revealed a direct relationship to the fraction of the unit cell occupied by the solvent. The significance of crystal contact is the displacement of the ligand molecule [39].

3.4. Cavity analysis

Cavity analysis (Table 2) was performed on the 1OE8 (Sh28GST) and 8ALS (Sb28GST) structures. Both structures exhibited two corresponding cavities each, as identified by spherical probes bearing radii bounds of 3–10 Å. The smaller cavity (Cavity 1) is at the dimer interface, with Cavity 2 existing within the adjoining glutathione and non-substrate binding sites (Figs. 6C and 6D). Overall, the cavities on the free structure were of more extensive volume and surface area.

3.5. Molecular dynamic simulation

Although 8ALS and 1OE8 share strong structural homology (Fig. 7), they vary in amino acid sequence at six positions. The six mutations (using 1OE8 as the wildtype) are V69L, G87E, E89D, A102V, Y110H and I124T, which indicates that 8ALS have extra charges compared to 1OE8 due to the presence of extra Glu87 and His110. Only one (V69L) of the variations occurred at the N-terminus thioredoxin domain containing the βαβαββα secondary structure architecture, th; theaining five mutations are in the C-terminus all-alpha helical domain. None of the six mutations is within 4 Å of the catalytic Tyr10. Following energy minimisation and systems preparations, the waters and the GSH ligand (in 1OE8) were stripped from the overall structures. Both systems were fully

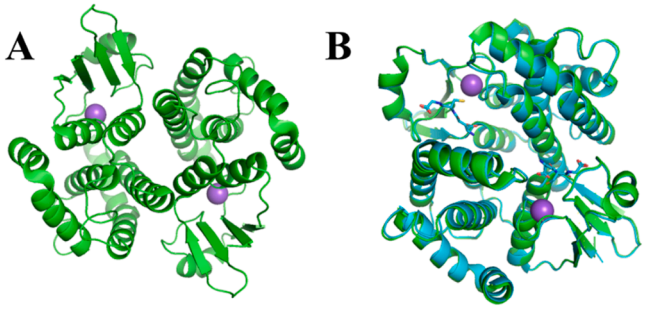

Fig. 4. Overall Sb28GST structure. (*A*) Sb28GST (PDB ID 8ALS). (*B*) Sb28GST (PDB ID 8ALS) superimposed with PDB ID 1OE8. The ribbon representations of the complexes reveal the two subunits (green) with a sodium atom (purple) and the GSH molecule (rainbow-coloured) for the superimposed structure only. The images were generated using PyMol.

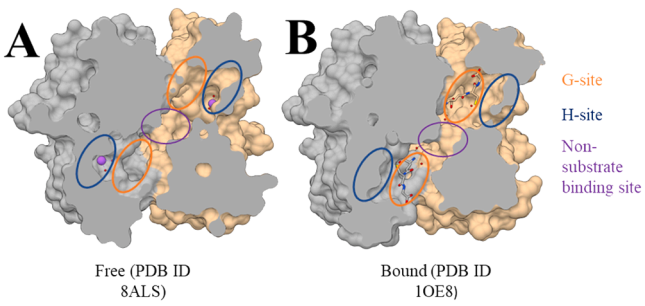

Fig. 5. Cross section of two structures of the 28 kDa GST dimer from (A) *S. bovis* (8ALS) and (B) *S. haematobium* (1OE8) showing the various binding sites. The bound structure (1OE8) is shown with glutathione in both G-sites.

Table 1
Data collection and refinement statistics.

Data collection	
Light source	Cu Kα
Wavelength (Å)	1.5418
Detector	Bruker D8 Venture Bio PHOTON III 28-pixel array area detector
Temperature (K)	100
Space group	$P\ 1\ 2_1\ 1$
Unit-cell parameters	
a, b, c (Å)	54.133, 77.086, 54.015
α, β, γ (°)	90.00, 93.15, 90.00
Resolution range (Å)	24.68 −2.30 (2.38–2.30) *
Number of observed reflections	158,575 (10,629) *
Number of unique reflections	19,612 (1752) *
Completeness (%)	98.8 (89.9) *
I/σ(I)	11.40 (3.40) *
†R_{merge}	0.132 (0.600) *
Multiplicity	8.1 (6.1) *
Structure refinement	
Reflection used	19,582
Resolution range	24.68–2.30
Final overall R_{factor} (%)	21.68
Rework (%) / ‡R_{free} (%)	21.52 / 24.48
Number of protein atoms	3274
Average B factor value (Å^2)	24.0
RMSD in bond length (Å)	0.002
RMSD in bond angles (°)	0.506
Ramachandran statistics	
Favoured; Allowed; Outliers (%)	96.00, 4.00, 0.00
Matthew's coefficient V_M (Å^{3}Da^{-1})	2.36
Solvent content (%)	47.98

compactthe the $R_{merg} = \sum_{hkl}\sum_{i}|I_i(hkl) - I(hkl)|/\sum_{hkl}\sum_{i}I_i(hkl)$, where *I(hkl)* is the intensity of reflection *hkl*, $\sum_{hkl}$ is the sum over all reflections and $\sum_{i}$ is the sum over *i* measurements of reflection hkl. ‡ R_{free} is calculated for a randomly chosen 5 % of reflections which were not used for refinement of the structure, and R_{work} is calculated for the remaining reflections.

Table 2
Cavity analysis of the 28-kDa GST structures shows two corresponding cavities. Cavity 1 exists within the dimer interface core of the enzyme, and cavity 2 occupies the adjoining G/H binding region.

Cavity	Parameter	8ALS	1OE8
1	Volume (Å^3)	507.00	321.00
	Surface area (Å^2)	393.00	254.00
	Effective radius (Å)	3.87	3.79
2	Volume (Å^3)	1690.00	708.00
	Surface area (Å^2)	1073.00	495.00
	Effective radius (Å)	4.72	4.29

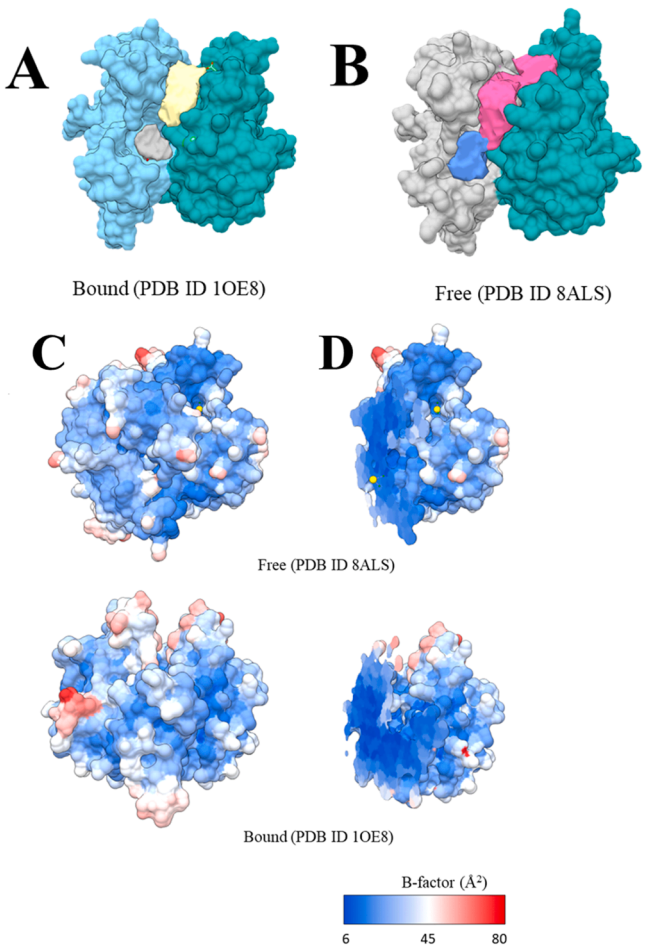

Fig. 6. Cavities in the (*A)* bound and (*B)* free Sb28GST. Molecular surface of (C) free and (D) bound Sb28GST coloured by the B-factor. The cross-section view is depicted across the dimer interface plane.

solvated using the TIP3P water model, and the net charge after solvation was zero because the charges were neutralised with counter ions (equivalent Na^+ or Cl^-). In addition, both systems were fully equilibrated for the MD simulation production. Hence, inferences can be made from both systems without bias.

The trajectory of the C^{α}, based on the RMSD (Fig. 8A), shows that the protein models exhibit different dynamics within the 1000 ns simulation time. The 8ALS model appears to be slightly more dynamic compared to 1OE8, with an average C^{α}-RMSD (±SD) of 2.95 Å (±0.32) and 2.09 Å (±0.17) for 8ALS and 1OE8, respectively. The C^{α}-RMSF trajectory substantiates this observation (Fig. 8B) derived within the 1000 ns simulation time. Our results suggest that the backbone of 8ALS fluctuated marginally more than the backbone of 1OE8 with an average (±SD) of 1.65 Å (±0.86) and 1.14 Å (±0.39) for 8ALS and 1OE8, respectively. Furthermore, the Cα-RMSF trajectory revealed that backbone fluctuation is not precisely identical across the two identical subunits. This variation in the backbone fluctuation is more pronounced at the C-terminus all alpha-helical domain (Fig. 8C) of this obligate homodimeric enzyme.

The radius of gyration (Rg), which may reflect the hydrodynamic volume of a globular protein, shows that 8ALS is less compact than 1OE8. This further confirms the variation in overall conformational dynamics as judged by the Cα-RMSD trajectory. The overall average Rg (±SD) for 8ALS and 1OE8 is 22.75 Å (±0.42) and 21.44 Å (±0.09), respectively. To further support our postulate that 8ALS is more dynamic than the 1EO8 model, we measured the distance between two atoms in helix 4 (α4), which forms part of the dimer interface topology. Using His110Cα and Asp89 C^{α} as reference atoms, we observed that the distance between the Cα of the two His110 (of the two subunits) fluctuated more in 8ALS than 1OE8; however, this was not the case for Asp89 C^{α} of the two subunits.

4. Discussion

Schistosomiasis is a tropical disease of poverty which ranks as the second cause of death amongst parasitic diseases [40]. The present study aimed to evaluate the unbound crystal structure of the 28-kDa isoform of GST from *Schistosoma bovis*. In this regard, protein crystal structures are essential since they highlight mechanisms of biological activities, thereby facilitating drug development to exploit protein function. The present study solved the crystal structures of unbound Sb28GST to provide insight into the proteins' structural conformations. Analysing the un-ligated form of Sb28GST enables the design of molecular compounds capable of selectively inhibiting the activity of Sb28GST.

The pET11a vector containing the full-length DNA sequence of Sb28GST was used to overexpress recombinant Sb28GST in the soluble cell fraction of *E. coli* cells. The purity of the Sb28GST samples was analysed using SDS-PAGE as described in Section 3.1. The purified protein sample exhibited an individual band corresponding to a subunit molecular mass of approximately 24 kDa on a 12.5 % SDS-PAGE gel (Fig. 1). The Protparam bioinformatics tool calculated the molecular weight directly by using the net isotopic mass of each amino acid to yield a theoretical value of 23.4 kDa [26]. Inconsistencies between the two molecular weights are due to the number of amino acids used in the Sb28GST sequence. Our structure is the only published structure of the 28-kDa S. bovis GST (Fig. 9).

The catalytic site consists of two ligand binding sites per subunit, namely the GSH-binding site (G-site) housed in the N-terminal domain and the hydrophobic xenobiotic binding site (H-site) found in the C-terminal domain [41]. The enzyme's catalytic activity was monitored through the enzyme's ability to catalyse the covalent conjugation of GSH to CDNB to form 1-(*S*-glutathionyl)−2, 4-dinitrobenzene (the product). The results obtained prove that Sb28GST is catalytically active. The specific activity of Sb28GST was obtained from the slope of a linear plot through the experimental data (Fig. 2A).

The secondary structural content of Sb28GST agrees with literature, which categorises cytosolic GSTs as predominantly alpha-helical [42]. The 222 nm/208 nm ratio of 8ALS to 1OE8 was reported to be 0.73 and 0.82, respectively, indicating that the secondary structure of Sb28GST comprised more coiled-coil α-helices. These differences in ellipticity amongst predominantly alpha-helical proteins depict the natural variation of the helices, thereby classifying them into coiled-coil helices or random coils if the 222 nm/208 nm ratio exists as ≥ 1 or ≤ 0.86, respectively [43]. This result confirmed that the integrity of the secondary structure of the enzyme was not compromised during recovery from the soluble *E. coli* cell fraction.

There are vast differences between the conformational changes of ligated and un-ligated GSTs in solution. Ligands can confer stability to proteins [44]. Both the Sb28GST (PDB 8ALS) and the Sb28GST (PDB 1OE8) are within the same space group of P21. In this case the ligand is not expected to induce significant conformational changes. The relevance of crystallising the apo form of the Sb28GST in this instance thus forms a basis for BSP binding. Evaluation of the crystal-packing parameter revealed that the lattice accommodates 2 biological molecules in the asymmetric unit. The Matthew's coefficient was 2.37 $Å^3$ Da^{-1} whilst the solvent content was 48.1 %. Further data-collection information is provided in Table 1.

The structural quality of the refined Sb28GST model was evaluated by monitoring the torsion angles of the polypeptide backbone conformation. The main chain angle orientations reveal that 97.28% falls within the preferred region of the Ramachandran plot, the residual 2.2% lies in the allowed region, and 0.42% occupies the less favourable generously allowed region. The protein structure has been deposited as

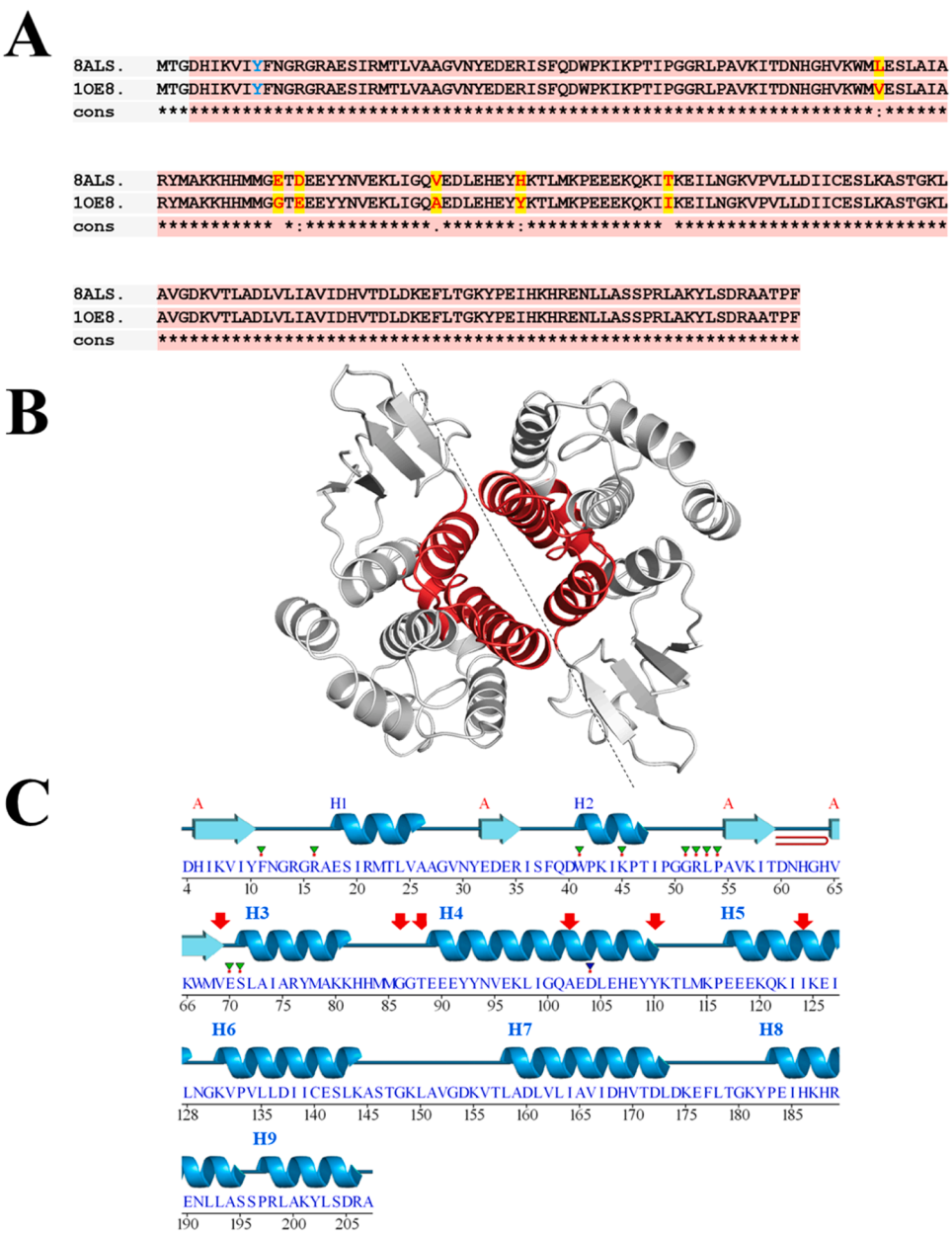

Fig. 7. Sequence analysis of 8ALS (Sb28GST) and 1OE8 (Sh28GST) showing the positions of the variant amino acids. (*A*) is a structural alignment of 8ALS and 1OE8 using Expresso™, which indicates the structural similarity between both protein models. (*B*) ribbon representation of 8ALS showing helix five and helix 6 (in red), which largely contributes to the dimer interface topography. (*C*) is the primary sequence analysis of 8ALS showing the position of the variant amino acids concerning the secondary structural elements.

entry 8ALS in the Protein Data Bank. The Sb28GST structure is dimeric in solution. This dimeric feature is also exhibited by other GST family members [45]. The model exhibits common GST features, such as the N and C terminals on the domain interface, with an additional sodium ion (Fig. 7). Monomers A and B comprised 204 residues. The two monomers look similar but exhibit very small similarities (Fig. 3B). Sb28GST encodes a catalytic Tyrosine residue found at position 10 (Tyr10) within the activating conformation position [25]. This active tyrosine site is mostly found in most cytosolic eukaryotic GSTs, specifically in the alpha, pi, mu, and sigma classes [25]. The Sb28GST under investigation in this study originates from the Sigma class. During the rotation process, it is anticipated that the catalytic tyrosine residue (Tyr10) of the sigma class Schistosoma haematobium wild-type glutathione-*S*-transferase will alternate between being within and without the binding site for reduced glutathione (referred to as the "G site"). When the tyrosine residue is in the outside position (Tyr10), it forms an π-cation interaction with the guanidinium group of Arg21 [21,22]. The enzyme displayed canonical GST characteristics. The RMSD between the two super imposed structures was as low as 0.418 Å (Fig. 4B).

Having observed the differences in amino acid composition between our model (8ALS) and the molecular replacement template (1OE8), we hypothesised that these six amino acid variations might impact the global structure of 8ALS. This implies that there may be variations in the structure and catalytic turnover rate of the 28 kDa-*S. haematobium* orthologue (8ALS) in comparison with 1OE8. Several studies have strongly correlated amino acid mutation in the form of substitution and insertions to enzyme variations in structure, dynamics, and kinetics [46–48]. Five of the six substitutions are on the predominantly alpha-helical C-terminus domain (Fig. 7). In contrast, the only substitution on the N-terminus domain appears to be withdrawn from the G

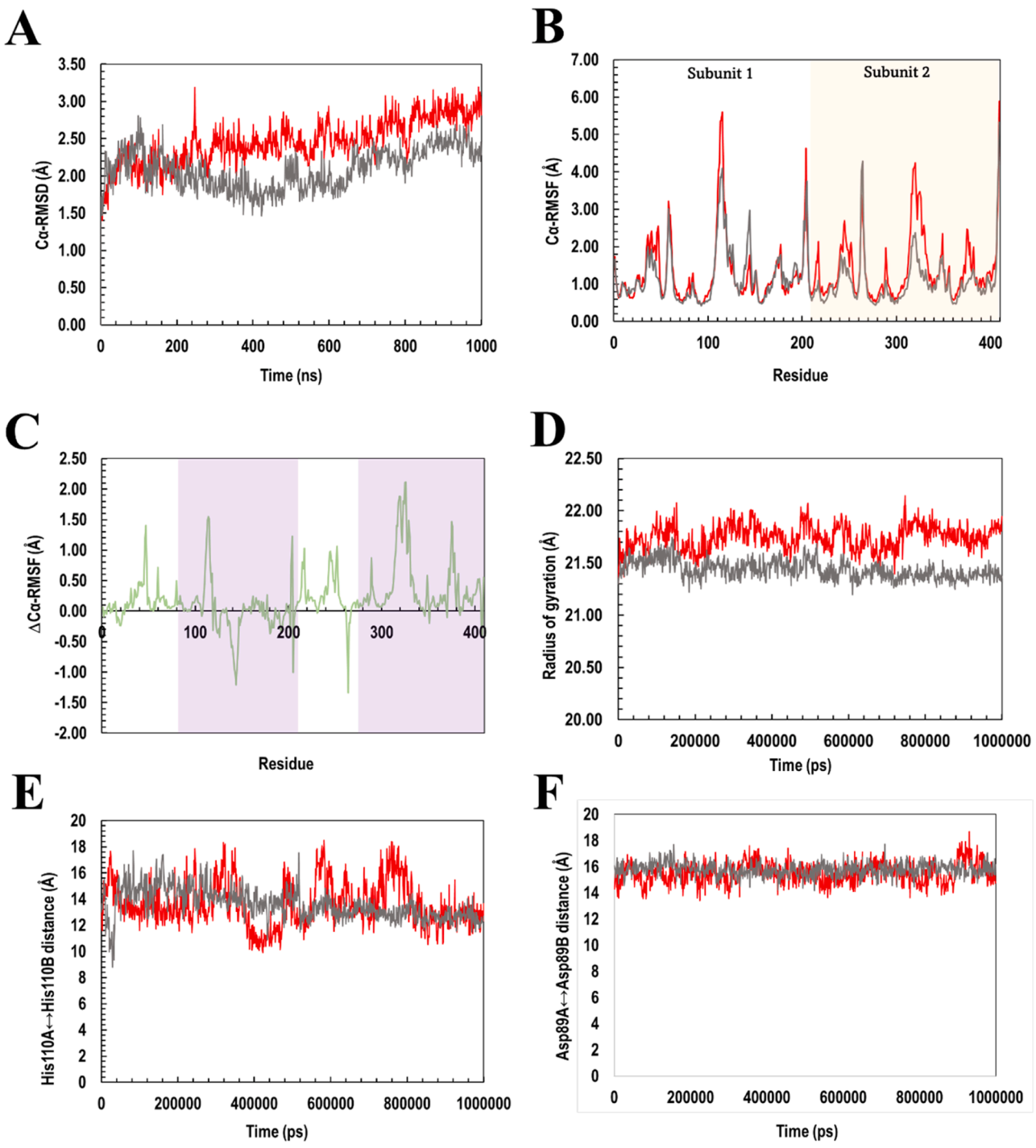

Fig. 8. Post-dynamic analysis of the molecular dynamic simulation of 8ALS (red profile) and 1OE8 (grey profile). Trajectories of the C^{α} showing the RMSD (*A*), RMSF (*B*), and changes in RMSF of 8ALS with reference to 1OE8 (*C*), Rg (*D*) and interatomic distances (*E* and *F*) were extracted and plotted as a function of the simulation time or residue numbers.

and H sites. The substitutions occurred mostly between α4 and α5, which are the two main helices of the dimer interface, which indicates that the variation may affect the hydrodynamic volume of this globular enzyme.

Although the variation may not seem to visibly induce any conformational changes in 8ALS compared to 1OE8, from the static structure point of view, we needed to use computational approach to unravel the structural landscape of the two proteins from an atomistic perspective. Therefore, it is crucial in this study's context to gain an atomistic interpretation of the variance in amino acid composition between what we postulate as isoenzymes of the 28-kDa *S. haematobium* GST. To support our theory, we used a 1000 ns molecular dynamics simulation to study the overall conformation of 8ALS in comparison with 1OE8 based on C^{α}-RMSD (alpha carbon), C^{α}-RMSF, the radius of gyration (Rg) and the distance between the corresponding catalytic atoms of the two subunits at the dimer interface. We supposed 1000 ns trajectory time is enough to explain our hypothesis based on the C^{α}-RMSD, C^{α}-RMSF, Rg and interdomain distance measurement. Molecular dynamic simulation of biological systems has shown relevance in interpreting empirical data. Although the crystallographic resolution may differ between these two model structures, we could still make reasonable extrapolations from

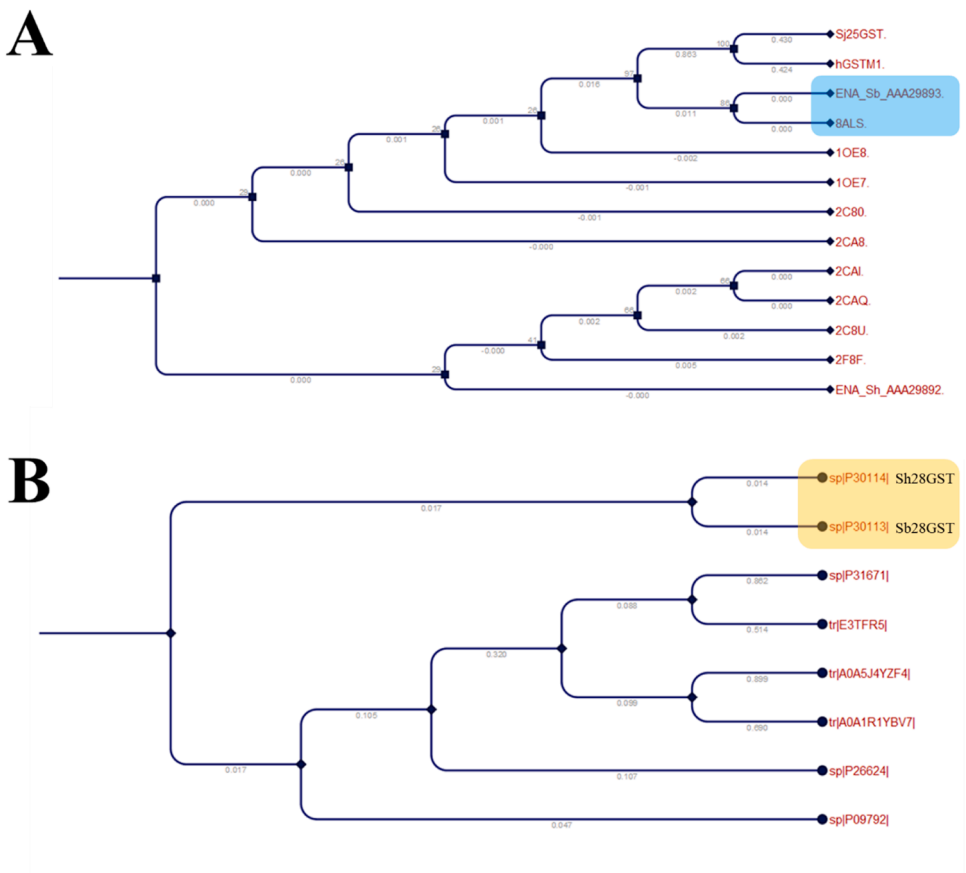

Fig. 9. Phylogenetic tree based on alignment of protein sequences. (*A*) is protein sequences of eight crystal structures of Sh28GST (2CAQ, 2F8F, 2CAI, 2CA8, 2C8U, 2C80, 1OE7, and 1OE8) and one structure (8ALS) of Sb28GST deposited in RCSB-PDB. The blue highlight shows that the only sequence deposited in the PDB closest to the Sb28GST sequence is 8ALS. (*B*) protein sequences of 28-kDa GST of various organisms extracted from the UniProtKB database. The gold highlight indicates how genetically close Sh28GST and Sb28GST are.

MD simulation data. Our results suggest that there may be variation in the overall dynamics and hydrodynamic volume of 8ALS concerning 1OE8. This may imply that the two proteins may have different kinetics but not in function. Hence, we can justifiably denote 8ALS as a variant of 1OE8 based on amino acid composition and enzyme kinetics.

We expected that this variation might also alter the dimer interface topology and the conformational stability of 8ALS. We measured the distance between the two dimers based on His110 and Asp89 inter-subunit distance as a function of the 1000 ns trajectory period. The results show that the distance between the dimers varies across the two proteins, suggesting that the variation in amino acid sequence alters the dimer interface's topology. This is corroborated by the dimer interface analysis results (Fig. 8), which show that the volume of the 8ALS dimer interface is more significant than that of the 1OE8. It is essential to mention that the dimer interface of GSTs plays a critical role in the structure and function of the enzyme, resulting in an altered hydrodynamic volume. GSTs are obligate dimers, except for *Plasmodium falciparum* GST, which shows tetramerisation in the absence of GSH but dimerises in the presence of GSH. Hence, any significant perturbation at the dimer interface, such as alteration in the distance between the subunits, may affect the kinetics propensity of the protein, such as turnover rate. It suffices to say that the variation in the amino acid across the two enzymes does not entirely alter the function but could affect the kinetics as well as stability of the enzyme. An empirical approach, such as chemical-induced equilibrium denaturation, would be needed to affirm this postulate.

In conclusion, we successfully over-expressed and purified the 28-kDa GST isoform from *Schistosoma bovis* and explored its structural and functional features alongside determining the crystal structure. The data obtained in this study is advantageous for the novel application of the un-ligated Sb28GST enzyme. In addition, the crystal structures obtained from the study provide a molecular basis for future evaluation in structure-based drug design of inhibitors with therapeutic potential against schistosomiasis. Future X-ray crystallographic studies on the liganded-Sb28GST studies will confirm the BSP binding site.

Declaration of Competing Interest

The authors declare the following financial interests/personal relationships which may be considered as potential competing interests:

Ikechukwu Achilonu reports financial support was provided by National Research Foundation of South Africa. Ikechukwu Achilonu reports financial support was provided by South African Medical Research Council.

Data availability

Data will be made available on request.

Acknowledgements

This work was supported by the South African Research Chairs Initiative (SARChI) of the Department of Science and Technology and National Research Foundation (grant 64788 to IA) and National Research Foundation. HM acknowledges the South African National Research Foundation for a scholarship toward her PhD degree. Authors thank the NRF and the University of the Witwatersrand for generous

funding to enable the purchase of a dual-wavelength hybrid diamond anode X-ray diffractometer (Bruker D8 Discovery Bio equipped with Mo and Cu X-ray sources) under NEP Grant No 129920. The authors also acknowledge the Centre for High-Performance Computing (CHPC), CSIR Cape Town, South Africa, for access to the Maestro molecular modelling suite.

Author contributions

Conceptualisation, IA, Methodology, HM, Validation, HM, original draft writing, HM and AV, Review and editing, I.A, RP and HM, Formal analysis, HM and AV, Crystallographic data collection and processing, RP, Structure solution and refinement, RP, Structure validation and deposition, RP, Resources, IA, Funding acquisition, IA, Project administration, IA

Credit Author Statement

Hattie Hope Makumbe: Performed all experimental studies including protein expression, purification, spectroscopic assays, crystallisation, solved the structure of the enzyme and also wrote and reviewed the manuscript. Ramesh Pandian: Performed the X-ray diffraction studies, collected the diffraction, and supervised the structure solution. Yasien Sayed, review the manuscript and provided critical comments that shaped the manuscript. Ikechukwu Achilonu: Conceptualized the study, designed the study, performed molecular dynamic simulation studies, validated the study, reviewed, and edited the manuscript.

References

[1] E. Raj, B. Calvo-Urbano, C. Heffernan, J. Halder, J. Webster, Systematic review to evaluate a potential association between helminth infection and physical stunting in children, Parasit Vectors 15 (1) (2022) 1–19.
[2] A.J. Oakley, M.L. Bello, M. Nuccetelli, A.P. Mazzetti, M.W. Parker, The ligandin (non-substrate) binding site of human Pi class glutathione transferase is located in the electrophile binding site (H-site), J. Mol. Biol. 291 (4) (1999) 913–926.
[3] Y. Temel, U.M. Koçyigit, M.Ş. Taysı, F. Gökalp, M.B. Gürdere, Y. Budak, M. Ceylan, İ. Gülçin, M. Çiftci, Purification of glutathione S-transferase enzyme from quail liver tissue and inhibition effects of (3aR, 4S, 7R, 7aS)-2-(4-((E)-3-(aryl) acryloyl) phenyl)-3a, 4, 7, 7a-tetrahydro-1H-4, 7-methanoisoindole-1, 3 (2H)-dione derivatives on the enzyme activity, J. Biochem. Mol. Toxicol. 32 (3) (2018) e22034.
[4] İ. Gülçin, A. Scozzafava, C.T. Supuran, Z. Koksal, F. Turkan, S. Çetinkaya, Z. Bingöl, Z. Huyut, S.H. Alwasel, Rosmarinic acid inhibits some metabolic enzymes including glutathione S-transferase, lactoperoxidase, acetylcholinesterase, butyrylcholinesterase and carbonic anhydrase isoenzymes, J. Enzyme Inhib. Med. Chem. 31 (6) (2016) 1698–1702.
[5] İ. Gülçin, A. Scozzafava, C.T. Supuran, H. Akıncıoğlu, Z. Koksal, F. Turkan, S. Alwasel, The effect of caffeic acid phenethyl ester (CAPE) on metabolic enzymes including acetylcholinesterase, butyrylcholinesterase, glutathione S-transferase, lactoperoxidase, and carbonic anhydrase isoenzymes I, II, IX, and XII, J. Enzyme Inhib. Med. Chem. 31 (6) (2016) 1095–1101.
[6] J.D. Hayes, J.U. Flanagan, I.R. Jowsey, Glutathione transferases, Annu. Rev. Pharmacol. Toxicol. 45 (1) (2005) 51–88.
[7] N. Allocati, M. Masulli, C. Di Ilio, L. Federici, Glutathione transferases: substrates, inihibitors and pro-drugs in cancer and neurodegenerative diseases, Oncogenesis 7 (1) (2018) 1–15.
[8] S. Vaish, D. Gupta, R. Mehrotra, S. Mehrotra, M.K. Basantani, Glutathione S-transferase: a versatile protein family, 3, BioTech 10 (7) (2020) 1–19.
[9] D. Sheehan, G. Meade, V.M. Foley, C.A. Dowd, Structure, function and evolution of glutathione transferases: implications for classification of non-mammalian members of an ancient enzyme superfamily, Biochem. J. 360 (1) (2001) 1–16.
[10] K. Turhan, B. Pektaş, F. Türkan, F.T. Tuğcu, Z. Turgut, P. Taslimi, H.S. Karaman, I. Gulcin, Novel benzo [b] xanthene derivatives: bismuth (III) triflate-catalyzed one-pot synthesis, characterization, and acetylcholinesterase, glutathione S-transferase, and butyrylcholinesterase inhibitory properties, Arch. Pharm. (Weinheim) 353 (8) (2020), 2000030.
[11] F. Türkan, Z. Huyut, P. Taslimi, M.T. Huyut, İ. Gülçin, Investigation of the effects of cephalosporin antibiotics on glutathione S-transferase activity in different tissues of rats in vivo conditions in order to drug development research, Drug Chem. Toxicol. 43 (4) (2020) 423–428.
[12] İ. Gulçin, P. Taslimi, A. Aygün, N. Sadeghian, E. Bastem, O.I. Kufrevioglu, F. Turkan, F. Şen, Antidiabetic and antiparasitic potentials: inhibition effects of some natural antioxidant compounds on α-glycosidase, α-amylase and human glutathione S-transferase enzymes, Int. J. Biol. Macromol. 119 (2018) 741–746.
[13] M.A. McTigue, D. Williams, J.A. Tainer, Crystal structures of a schistosomal drug and vaccine target: glutathione S-transferase from Schistosoma japonica and its complex with the leading antischistosomal drug praziquantel, J. Mol. Biol. 246 (1) (1995) 21–27.
[14] K.A. O'Leary, J.W. Tracy, Schistosoma mansoni: glutathione S-transferase-catalyzed detoxication of dichlorvos, Exp. Parasitol. 72 (4) (1991) 355–361.
[15] D.M. Townsend, K.D. Tew, The role of glutathione-S-transferase in anti-cancer drug resistance, Oncogene 22 (47) (2003) 7369–7375.
[16] N. Vale, M.J. Gouveia, G. Rinaldi, P.J. Brindley, F. Gärtner, J.M. Correia da Costa, Praziquantel for schistosomiasis: single-drug metabolism revisited, mode of action, and resistance, Antimicrob. Agents Chemother. 61 (5) (2017) e02582. -16.
[17] A. Oakley, Glutathione transferases: a structural perspective, Drug Metab. Rev. 43 (2) (2011) 138–151.
[18] W.H. Habig, M.J. Pabst, W.B. Jakoby, Glutathione S-transferases: the first enzymatic step in mercapturic acid formation, J. Biol. Chem. 249 (22) (1974) 7130–7139.
[19] G. Litwack, B. KETTERER, I.M. ARIAS, Ligandin: a hepatic protein which binds steroids, bilirubin, carcinogens and a number of exogenous organic anions, Nature 234 (5330) (1971) 466–467.
[20] D. Kolobe, Y. Sayed, H.W. Dirr, Characterization of bromosulphophthalein binding to human glutathione S-transferase A1-1: thermodynamics and inhibition kinetics, Biochem. J. 382 (2) (2004) 703–709.
[21] J. Newman, L. Pearce, C.A. Lesburg, C. Strickland, T.S. Peat, Crystallization of an apo form of human arginase: using all the tools in the toolbox simultaneously, Acta Crystallogr. Sect. F Struct. Biol. Cryst. Commun. 67 (1) (2011) 90–93.
[22] T.K. Hitchens, B. Mannervik, G.S. Rule, Disorder-to-order transition of the active site of human class Pi glutathione transferase, GST P1-1, Biochemistry 40 (39) (2001) 11660–11669.
[23] G. Ricci, A.M. Caccuri, M.L. Bello, N. Rosato, G. Mei, M. Nicotra, E. Chiessi, A. P. Mazzetti, G. Federici, Structural flexibility modulates the activity of human glutathione transferase P1-1: role of helix 2 flexibility in the catalytic mechanism, J. Biol. Chem. 271 (27) (1996) 16187–16192.
[24] L. Stella, A.M. Caccuri, N. Rosato, M. Nicotra, M.L. Bello, F. De Matteis, A. P. Mazzetti, G. Federici, G. Ricci, Flexibility of helix 2 in the human glutathione transferase P1-1: time-resolved fluorescence spectroscopy, J. Biol. Chem. 273 (36) (1998) 23267–23273.
[25] K.A. Johnson, F. Angelucci, A. Bellelli, M. Hervé, J. Fontaine, D. Tsernoglou, A. Capron, F. Trottein, M. Brunori, Crystal structure of the 28kDa glutathione S-transferase from Schistosoma haematobium, Biochemistry 42 (34) (2003) 10084–10094.
[26] E. Gasteiger, C. Hoogland, A. Gattiker, M.R. Wilkins, R.D. Appel, A. Bairoch, Protein identification and analysis tools on the ExPASy server, The proteomics protocols handbook (2005) 571–607.
[27] M.O. Karaytuğ, N. Balcı, F. Türkan, M. Gürbüz, M.E. Demirkol, Z. Namlı, L. Tamam, İ. Gülçin, Piperazine derivatives with potent drug moiety as efficient acetylcholinesterase, butyrylcholinesterase, and glutathione S-transferase inhibitors, J. Biochem. Mol. Toxicol. 37 (2) (2023) e23259.
[28] P. Taslimi, M. Işık, F. Türkan, M. Durgun, C. Türkeş, İ. Gülçin, Ş. Beydemir, Benzenesulfonamide derivatives as potent acetylcholinesterase, α-glycosidase, and glutathione S-transferase inhibitors: biological evaluation and molecular docking studies, J. Biomol. Struct. Dyn. 39 (15) (2021) 5449–5460.
[29] Bruker, PROTEUM4 version 2021.4-1 data collection software which includes SAINT version 8.40B, SADABS-2016/2 and XPREP version 2014/2, in: B. USA (Ed.) Bruker AXS Inc., Madison, Wisconsin, USA., 2021.
[30] Z. Otwinowski, W. Minor, D. Borek, M. Cymborowski, Denzo and scalepack, (2012).
[31] P.R. Evans, An introduction to data reduction: space-group determination, scaling and intensity statistics, Acta Crystallogr. D 67 (4) (2011) 282–292.
[32] P. Evans, Scaling and assessment of data quality, Acta Crystallogr. D 62 (1) (2006) 72–82.
[33] A.J. McCoy, R.W. Grosse-Kunstleve, P.D. Adams, M.D. Winn, L.C. Storoni, R. J. Read, Phaser crystallographic software, J. Appl. Crystallogr. 40 (4) (2007) 658–674.
[34] P. Emsley, K. Cowtan, Coot: model-building tools for molecular graphics, Acta Crystallogr. D 60 (12) (2004) 2126–2132.
[35] P.V. Afonine, R.W. Grosse-Kunstleve, N. Echols, J.J. Headd, N.W. Moriarty, M. Mustyakimov, T.C. Terwilliger, A. Urzhumtsev, P.H. Zwart, P.D. Adams, Towards automated crystallographic structure refinement with phenix. refine, Acta Crystallogr. D 68 (4) (2012) 352–367.
[36] R.A. Laskowski, M.W. MacArthur, D.S. Moss, J.M. Thornton, PROCHECK: a program to check the stereochemical quality of protein structures, J. Appl. Crystallogr. 26 (2) (1993) 283–291.
[37] L. Whitmore, B. Wallace, DICHROWEB, an online server for protein secondary structure analyses from circular dichroism spectroscopic data, Nucleic. Acids. Res. 32 (suppl_2) (2004) W668–W673.
[38] A. Vagin, A. Teplyakov, MOLREP: an automated program for molecular replacement, J. Appl. Crystallogr. 30 (6) (1997) 1022–1025.
[39] J. Luo, Z. Liu, Y. Guo, M. Li, A structural dissection of large protein-protein crystal packing contacts, Sci. Rep. 5 (1) (2015) 1–13.
[40] A.F. Adenowo, B.E. Oyinloye, B.I. Ogunyinka, A.P. Kappo, Impact of human schistosomiasis in sub-Saharan Africa, Brazil. J. Infect. Dis. 19 (2015) 196–205.
[41] S. Mohsenzadeh, M. Esmaeili, F. Moosavi, M. Shahrtash, B. Saffari, H. Mohabatkar, Plant glutathione S-transferase classification, structure and evolution, Afr. J. Biotechnol. 10 (42) (2011) 8160–8165.
[42] S. Gildenhuys, M. Dobreva, N. Kinsley, Y. Sayed, J. Burke, S. Pelly, G.P. Gordon, M. Sayed, T. Sewell, H.W. Dirr, Arginine 15 stabilizes an SNAr reaction transition state and the binding of anionic ligands at the active site of human glutathione transferase A1-1, Biophys. Chem. 146 (2–3) (2010) 118–125.

[43] S. Lau, A. Taneja, R. Hodges, Synthesis of a model protein of defined secondary and quaternary structure. Effect of chain length on the stabilization and formation of two-stranded alpha-helical coiled-coils, J. Biol. Chem. 259 (21) (1984) 13253–13261.
[44] A.M. Hassell, G. An, R.K. Bledsoe, J.M. Bynum, H.L. Carter, S.J. Deng, R.T. Gampe, T.E. Grisard, K.P. Madauss, R.T. Nolte, Crystallization of protein–ligand complexes, Acta Crystallogr. D 63 (1) (2007) 72–79.
[45] R.N. Armstrong, Structure, catalytic mechanism, and evolution of the glutathione transferases, Chem. Res. Toxicol. 10 (1) (1997) 2–18.
[46] J.L. Radkiewicz, C.L. Brooks, Protein dynamics in enzymatic catalysis: exploration of dihydrofolate reductase, J. Am. Chem. Soc. 122 (2) (2000) 225–231.
[47] J.R. Schnell, H.J. Dyson, P.E. Wright, Structure, dynamics, and catalytic function of dihydrofolate reductase, Annu. Rev. Biophys. Biomol. Struct. 33 (2004) 119–140.
[48] P.K. Agarwal, Enzymes: an integrated view of structure, dynamics and function, Microb. Cell Fact. 5 (2006) 1–12.